

Small-angle neutron scattering and Molecular Dynamics structural study of gelling DNA nanostars

J. Fernandez-Castanon,¹ F. Bomboi,¹ L. Rovigatti,^{2,3} M. Zanatta,⁴ A. Paciaroni,⁴ L. Comez,^{4,5} L. Porcar,⁶ C. J. Jafra,⁷ G. C. Fadda,⁸ T. Bellini,⁹ and F. Sciortino^{1,10, a)}

¹⁾ *Sapienza–Università di Roma, P.le A. Moro 5, 00185 Roma, Italy*

²⁾ *Rudolf Peierls C. T. P., University of Oxford, 1 Keble Road, Oxford, OX1 3NP, United Kingdom*

³⁾ *Faculty of Physics, University of Vienna, Boltzmannngasse 5, A-1090 Vienna, Austria*

⁴⁾ *Dipartimento di Fisica, Università di Perugia, Via Pascoli, 06123 Perugia, Italy*

⁵⁾ *IOM-CNR, UOS Perugia c/o Dipartimento di Fisica e Geologia, Università di Perugia, Via Pascoli, 06123 Perugia, Italy*

⁶⁾ *Institut Laue-Langevin, 71 avenue des Martyrs, CS 20156, 38042 Grenoble cedex 9, France*

⁷⁾ *Helmholtz-Zentrum Berlin, Hahn-Meitner-Platz 1, 14109 Berlin, Germany*

⁸⁾ *Laboratoire Léon Brillouin, LLB, CEA Saclay, 91191 Gif-sur-Yvette Cedex, France*

⁹⁾ *Department of Medical Biotechnology and Translational Medicine, Università di Milano, I-20133 Milano, Italy*

¹⁰⁾ *CNR-ISC, UOS Sapienza–Università di Roma, I-00186 Roma, Italy*

(Dated: 28 August 2018)

DNA oligomers with properly designed sequences self-assemble into well defined constructs. Here, we exploit this methodology to produce bulk quantities of tetravalent DNA nanostars (each one composed by 196 nucleotides) and to explore the structural signatures of their aggregation process. We report small-angle neutron scattering experiments focused on the evaluation of both the form factor and the temperature evolution of the scattered intensity at a nano star concentration where the system forms a tetravalent equilibrium gel. We also perform molecular dynamics simulations of one isolated tetramer to evaluate the form factor theoretically, without resorting to any approximate shape. The numerical form factor is found to be in very good agreement with the experimental one. Simulations predict an essentially temperature independent form factor, offering the possibility to extract the effective structure factor and its evolution during the equilibrium gelation.

Keywords: Gels, DNA, Small-Angle Neutron Scattering, self-assembling

I. INTRODUCTION

The development of new *smart nanomaterials*^{1,2}, which are able to adapt their response to different external stimuli at the nanoscale, paves the way for the future of fields as diverse as medicine^{3–5}, drug-delivery^{6–8}, photonics^{9,10} and computing^{11,12}, among others. The deoxyribonucleic acid (DNA) is one of the most promising materials to encompass all of the aforementioned applications due to its base pairing specificity (A...T, G...C) which allows for absolute control over the design of deliberated structures. The responsible of storing our genetic information, something as natural as life itself, startlingly provides the perfect ingredient to create new functional materials^{13,14} via a cascade of self-assembly processes, each one guided by the length of complementary sequences of distinct DNA strands.

One of the first DNA constructs which has been designed and realized in the lab¹⁵ is the DNA nanostar (NS) with controlled valence f . To build the structure, f properly designed DNA single strands are mixed together in equimolar concentrations.

The sequence design favours the pairing of each strand with two different partners, in such a way that a construct with a flexible, unpaired core and f double-helical

arms structure is spontaneously formed (see Fig. 1). A self-complementary short sequence at the end of each arm provides the sticky site to bind distinct NSs. This methodology allows for the synthesis of supramolecular constructs in bulk quantities, opening the way for an experimental study of their bulk behavior. NS particles have been selected as optimal candidates for testing the role of the valence on the gas-liquid phase separation^{16,17}. Consistent with theoretical studies^{18,19} it has been shown that these particles undergo a phase-separation process between a phase of isolated NS and a network phase, in which NS particles bind to form a thermoreversible gel, the physical analog of f -functional chemical gels²⁰.

Differently from the chemical analog, the equilibrium phase behavior of this system can be explored. Beyond the coexisting density, on cooling, the system moves continuously from a high- T state in which monomers only interact via their excluded volume (and eventually electrostatic) repulsion to a fully bonded low temperature state (the equilibrium gel) via a progressive formation of larger and larger aggregates. The possibility to break and reform bonds makes it possible to release stresses and reach at low T a fully bonded state, e.g. a gel free of entanglement and defects.

Dynamic light scattering (DLS) experiments^{17,21} of the DNA-gel formation have shown that the density fluctuations relax slower and slower on cooling, following an Arrhenius T dependence, increasing by more than five

^{a)} Electronic mail: francesco.sciortino@phys.uniroma1.it

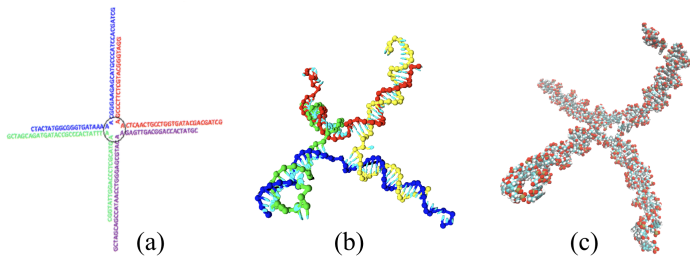


FIG. 1. Representation of a NS at different levels. (a) The four sequences of bases forming the NS. Each single strand has been represented with a different color. Note the six unpaired bases, acting as sticky ends (b) the oxDNA representation of the self-assembled NS, in which each base is modelled as a rigid body; (c) the corresponding full atom representation.

orders of magnitude in a small T interval, before exiting from the accessible experimental time window (10 seconds). Here, we present a series of Small-Angle Neutron Scattering (SANS) experiments carried out to quantify the structural signatures associated with the formation of the equilibrium gel at a suitably selected concentration as a function of T . At this concentration, the system evolves from fluid to gel through a succession of equilibrium steps, without the interference of phase separation. We also present experiments at a much lower concentration, where the form factor of the NS can be measured. We complement the experimental study with a numerical investigation of the structure of a single NS, based on the coarse-grained oxDNA²² model. This provides an effective way to connect the observed signatures in the SANS diffraction pattern with geometrical parameters. The quality of the experimental data and the agreement with the theoretical evaluation of the form factor allow us to extract an effective structure factor between the centers of the NSs under the hypothesis of decoupling between translational and orientational degrees of freedom.

II. MATERIALS AND METHODS

Materials and Sample preparation

The four sequences programmed to self-assemble in tetravalent DNA-NSs are:

Sequence 1. 5'-CTACTATGGCGGGTGATAAAA
CGGGAAGAGCATGCCATCCACGATCG-3'

Sequence 2. 5'-GGATGGGCATGCTCTTCCCGAA
CTCAACTGCCTGGTGATACGACGATCG-3'

Sequence 3. 5'-CGTATCACCAGGCAGTTGAGAA
CATGCGAGGGTCCAATACCGACGATCG-3'

Sequence 4. 5'-CGGTATTGGACCCCTCGCATGAA
TTTATCACCCGCCATAGTAGACGATCG-3'

where sequences with the same color indicate comple-

mentary strands. The red AA bases at the center of each sequence constitute the central flexible core. The black (CGATCG) self-complementary 6-bases overhangs provide the sequences that permit the connection between different DNA-NS via so-called *sticky-ends*. Bonding between different DNA-NS is favoured by the inclusion of a nucleotide A immediately before the sticky-end. The non-bonded sequences help releasing angular and rotational constraints, permitting both arm bending and rotation of the end sequences. Depending on the salt-concentration, NSs form at relatively high T and the lifetime of the aggregates becomes essentially infinite at ambient and smaller T . In our case, NSs self-assemble around 65°C and start to bind to each other below 50°C¹⁶.

We prepare the sample dissolving each of the four DNA single strands (provided by IDT and purified in a polyacrylamide gel (PAGE)) in deionized and degassed filtered (0.2 μm filters) H₂O water. Each sample is then centrifuged at 25 °C / 4.4 rpm for 5 minutes to favour the powder dissolution. Up to three different Nanodrop²³ measurements are undertaken to obtain accurate values of the strand concentration. The absorbance measurements (ratios 260/280 = 1.89 and 260/230 = 2.27) confirm the absence of proteins and low concentrations of other contaminants. The resulting solutions are then mingled at proper mixing ratios in order to obtain an equimolar solution of the four different strands. The prepared final concentration was 21 mg/ml, corresponding to 348 μM of NS. Assuming that each phosphate group releases one counter ion, then $[\text{Na}^+] \approx 63 \text{ mM}$. The experimental form factor of the DNA-NS required the preparation of a more diluted sample at $c = 3.2 \text{ mg ml}^{-1}$ (53 μM DNA-NS). The diluted sample was prepared in an electrolyte 63 mM NaCl solution to mimic the Na release conditions of the high concentrated sample. This DNA concentration meets the requirements to provide a signal strong enough, and consequently a good statistics in the SANS measurements, but at the same time to reduce to the minimum the inter-particle interactions. The resulting samples are heated at 90°C for 20 minutes and then cooled down to room temperature in about 7 hours. Further details on the preparation can be found in Ref. 17.

Small-Angle Neutron Scattering experiments

Comparable volumes, 80 μl , of the two samples (low and high concentrations) were prepared to fill up the quartz Hellma cells (0.5 mm path).

SANS measurements of the high concentrated sample were performed at the small-angle diffractometer $D22$ of the Institut Laue Langevin [DOI: 10.5291/ILL-DATA.9-13-559] (ILL, Grenoble, France)^{24,25}. Measurements were done at different temperature, ranging from 55°C to 5°C. Immediately before the data acquisition, we let the samples thermalize for 25 minutes at each temperature. Ex-

exploiting the ILL's high flux reactor, measurements of 5, 20 and 30 minutes were respectively taken at three sample-detector distances $L_{SD} = 1.40$ m, $L_{SD} = 5.60$ m and $L_{SD} = 17.00$ m. This instrument configuration, together with the incident neutron wavelength $\lambda_0 = 6$ Å selected, allowed us to cover a wavevector, q , window ranging from 0.0025 to 0.6 \AA^{-1} .

The raw data were treated according to standard procedures, including solvent and empty cell subtraction, using GRASP software provided by ILL²⁶, which yields the value of the scattering intensity onto the absolute intensity scale.

The same sample was also probed at the SANS instrument PACE of the Laboratoire Léon Brillouin (LLB, CEA Saclay, France). The instrument configuration allowed to cover a q -range from 0.02 to 0.6 \AA^{-1} . This was obtained with three setups, using an incident neutron wavelength $\lambda_0 = 5$ Å combined to $L_{SD} = 1.00$ m and $L_{SD} = 3.00$ m, and with $\lambda_0 = 12$ Å and $L_{SD} = 3.00$ m to reach the smallest q -values. In order to get a good signal-to-noise ratio, an acquisition time of 30 minutes was necessary for the first two cases, extending it up to 60 minutes for the last one. To test the reversibility of the assembling process of our system, three measurements were taken at $T = 20^\circ\text{C}$. Starting from 20°C , the sample was heated up to 45°C , cooled down back to 20°C , then to 6°C , and finally heated up again to 20°C . Each measurement was performed after a thermalization time of 20 minutes. The data were analysed with the software PASiNET.

Finally, for the purpose of properly evaluate the form factor $P(q)$, the more diluted sample was measured at the V4 instrument of the neutron source BER II at the Helmholtz-Zentrum Berlin facilities (HZB, Berlin, Germany)²⁷. After 40 minutes of sample thermalization at 50°C , rather long measurements of about 3 hours, about 7 hours, and 19 hours were acquired at $L_{SD} = 1.35$ m, $L_{SD} = 4.00$ m and $L_{SD} = 16.00$ m, respectively. These sample-detector distances, coupled to an incident wavelength $\lambda_0 = 6$ Å, allow to cover a q -range of $0.01 < q < 0.39 \text{ \AA}^{-1}$, equivalent to the one investigated on D22. Standard data reduction was accomplished by means of the BerSANS-PC software²⁸.

Deuteration, either of the solvent or of the sample, is a typical procedure when dealing with biological samples. Typically, the exchange of hydrogen with deuterium atoms permits to exploit the advantages of contrast variation in SANS experiments, and thus to clearly discriminate between the buffer and the sample. However, in this case, no contrast investigations were required. In fact, the little amount of H atoms found in DNA when compared to proteins and lipids, allowed us to use H_2O as a solvent to achieve the best contrast condition, while removing most of the strong ^1H incoherent background via a careful buffer subtraction, retaining a good statistics for the scattered signal.

III. SIMULATIONS

We perform molecular dynamics simulations of one isolated NS for different T and salt concentrations to provide theoretical predictions for the NS form factor. We employ oxDNA2²⁹, a coarse-grained model that has been shown to provide a physical representation of the thermodynamic and mechanical properties of single- and double-stranded DNA^{22,30,31}. The basic unit of the model is a nucleotide, represented as an oriented rigid body. In oxDNA2, the interaction between nucleotides takes into account the sugar-phosphate backbone connectivity, excluded volume, hydrogen bonding, nearest neighbour stacking, cross-stacking between base-pair steps in a duplex and coaxial stacking. Hydrogen bonding can occur between complementary bases when they are antialigned, leading to the formation of double-stranded conformations. Electrostatic interactions are included as screened Yukawa repulsions, assuming dissociation of the phosphorous sites.

In order to evaluate the form factor of the NS, we first need to convert the oxDNA2 representation into a full-atom one. This conversion is crucial to properly reproduce the interatomic distances and therefore their scattering signature in the large q window. We carry out this procedure by considering that the orientation of each coarse-grained base is identified by three axes. Two of these, \vec{a}_1 and \vec{a}_3 , define the directions along which hydrogen bonding and stacking interactions are maximised. These can be mapped onto an aromatic base by exploiting the planarity of the latter, making it possible to define the atomic analogues of \vec{a}_1 and \vec{a}_3 . This procedure fixes the orientation of the bases. Their positions are then set by superimposing the base site of each coarse-grained nucleotide with the centre of mass of the full-atom aromatic ring and shifting it by 1.13 Å. When applied to a perfect double helix, this method reproduces the full-atom phosphate-phosphate distances with a 99.9% accuracy.

We evaluate the numerical form factor $P(\mathbf{q})$ as the modulus

$$P(\mathbf{q}) \equiv \langle |F_{NS}(\mathbf{q})|^2 \rangle \quad (1)$$

where

$$F_{NS}(\mathbf{q}) \equiv \sum_{j=1}^N b_j \exp[i\mathbf{q} \cdot \mathbf{t}_j], \quad (2)$$

N is the total number of atoms composing the NS, \mathbf{t}_j is the vector joining the center of mass of the NS to atom j and b_j the atom scattering length³². The average $\langle \dots \rangle$ is performed over all different orientations and all different configurations generated in the molecular dynamics run (to sample all possible geometrical shapes assumed by the NS). We also evaluate

$$F(\mathbf{q}) \equiv \langle F_{NS}(\mathbf{q}) \rangle^2 \quad (3)$$

a quantity requested to estimate the quality of the orientational decoupling^{33,34}.

IV. RESULTS AND DISCUSSION

A. Dilute sample: Form Factor analysis

Fig. 2 shows the normalized intensity measured at $T = 50^\circ\text{C}$ for the sample at $c = 3.2$ mg/ml, compared with the form factor $P(q)$ calculated numerically from the NS generated via the oxDNA2 potential²⁹, with full-atom substitution. Beyond 0.03 \AA^{-1} , the experimental data are very well described by the theoretical function, supporting the quality of the oxDNA force-field in modelling the structure of the NS. The gyration radius, calculated by the atomic model, correspond to $R_g = 54 \text{ \AA}$, to be compared with an estimated length of the double helix arms of 68 \AA (3.4 \AA for 10 bases³⁵). Fig. 2 also shows the theoretical form factor of a homogeneous rigid cylinder with length much larger than the diameter ($2r_c$)^{36,37}

$$P(q) \sim \left(\frac{2J_1(qr_c)}{qr_c} \right)^2 \quad (4)$$

where J_1 is the Bessel function of the first kind. Between $0.1 \text{ \AA}^{-1} < q < 0.35 \text{ \AA}^{-1}$ the signal from the cylindrical shape of the DNA arms is prominent. Indeed, in this q -vector window, the experimental data can be quite accurately modeled by the form factor of a homogeneous rigid cylinder of radius 8 \AA . This cross-section radius agrees with the value reported in previous small-angle scattering studies of DNA short double helices^{38–40}. We ascribe the difference between such a value and the outer diameter of the B-DNA helix ($\sim 10 \text{ \AA}$) to the assumption of homogeneous cylinder^{41–45}.

For $q < 0.03 \text{ \AA}^{-1}$, the experimental form factor shows deviations from the simulated one, signalling the presence of a repulsive interaction between the NS, possibly originated by the screened electrostatic repulsion. Indeed, DNA is known to be a highly negatively charged polymer, in which all phosphorous groups are ionised, resulting in a bare net charge of about $200 e$ per tetramer. The significant DNA charge originates an inter-NS repulsion significantly larger than the thermal energy, resulting to a first approximation in an expanded double helix diameter³⁸. A precise characterization of this low q window would require measurements at lower NS concentrations, where, unfortunately, experiments are not easily performed due to the weak scattering signal.

The quality of the comparison between the experimental and theoretical structure factor, beside providing a precise characterisation of the geometry of the NS, confirms the high efficiency of the self-assembly process. Electrophoretic gel runs have indeed suggested that more than 95 per cent of the NS properly form¹⁶.

The agreement between simulations and experimental data offers us the possibility to exploit simulations to quantify the dependence of the NS radius of gyration, R_g on T and on the salt concentration. The T -dependence is particularly relevant, since it is not possible to perform

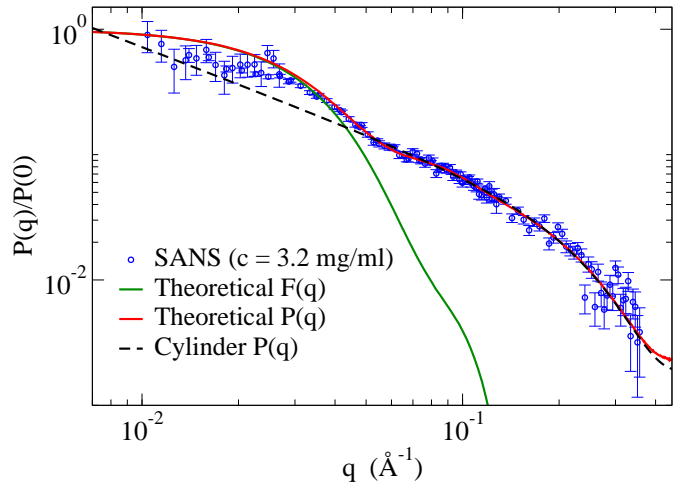


FIG. 2. Normalized form factor $P(q)$. Experimental SANS (blue dots) and simulated (solid red line) form factor at 50°C as a function of q in log-log scale. $P(q)$ of an infinite long cylinder with cross section radius $R_c = 8 \text{ \AA}$ from Eq. 4 (dashed black line). The figure shows also $F(q)$ from Eq. 3 (solid green line). The numerical $P(q)$ and $F(q)$ are calculated averaging over an equilibrium ensemble of configurations of an isolated NS at 50°C and $[\text{NaCl}] = 0.1 \text{ M}$.

experiments at low T at dilute concentration due to the onset of the limited-valence gas-liquid like phase separation¹⁶ which takes place in the sample. Luckily, the inset of Fig. 3 reveals that R_g strongly depends on the salt concentration whereas it weakly changes with T . According to the oxDNA2 model, the increase of R_g arises prevalently from the expansion of the central junction, where repulsive forces are non compensated by complementary base bonding. The predicted salt dependence of $P(q)$ shows the sensitivity of the experimental measurement, which is only consistent with the form factor evaluated at the lowest accessible ionic strength²⁹.

B. Gel-forming sample

Previous static and dynamic light scattering studies have focused on the thermodynamic behavior of the NS, providing evidence of a limited-valence phase separation¹⁶ in the low concentration region. At a total $[\text{Na}^+] \approx 60 \text{ mM}$, phase separation extends from very low concentration up to 17 mg/ml . For higher NS concentration the system remains homogeneous at all temperatures, forming an open equilibrium-gel structure at low T ¹⁶.

We provide here the first measurement of the structural properties of the system in the equilibrium gel region, covering the range of T (from 55°C to 5°C) over which

DLS observes an increase of the relaxation time by more than five orders of magnitude, revealing the formation of larger and larger clusters of bonded NSs that eventually span the entire system, forming the gel. The highest investigated T is lower than the temperature at which the stars unfold ($T_m \approx 65^\circ\text{C}$).

The scattered intensity provides a measure of the space pair correlation, weighted by the atomic scattering length. Formally, for a system of N_S nanostars, the q -dependence of the signal, is defined as^{33,46}

$$I(\mathbf{q}) \equiv \frac{1}{N_S} \left\langle \sum_{l=1}^{N_S} \sum_{m=1}^{N_S} \exp[i\mathbf{q} \cdot (\mathbf{r}_{CM}^l - \mathbf{r}_{CM}^m)] F_l(\mathbf{q}) F_m^*(\mathbf{q}) \right\rangle \quad (5)$$

where \mathbf{r}_{CM}^l indicates the center of mass position of the l -th NS and $F_l(\mathbf{q})$ is the previously defined F_{NS} function (see Eq. 2) for the l -th NS.

Experimentally, the differential cross-section $d\sigma$ per solid angle $d\Omega$ is defined as

$$\left(\frac{d\sigma}{d\Omega} \right)_{NS}(\mathbf{q}) = \beta I(\mathbf{q}) \quad (6)$$

where $\beta = nv_p^2(\Delta\rho)^2$, with n the number density of particles, v_p the volume occupied by a NS, and $\Delta\rho$ the particle scattering length density difference between NS and solvent.

Since we have measured the solvent contribution only at one temperature, we have estimated the scattered intensity from the system of DNA NSs, $(\frac{d\sigma_c}{d\Omega})_{NS}(q)$, at the different T by subtracting from the measured intensity, $I_m = (\frac{d\sigma_c}{d\Omega})_m(q)$, the solvent scattering, $I_s = (\frac{d\sigma_c}{d\Omega})_s(q)$, multiplied by a fitting T -dependent factor α . The best

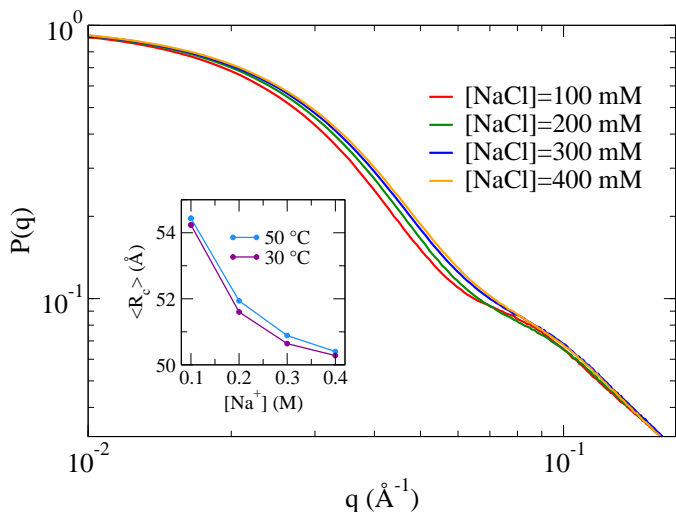


FIG. 3. Theoretical predictions for the ionic strength dependence of the form factor based on the oxDNA2 model. The inset shows the corresponding gyration radii R_g for two different T as a function of salt concentration.

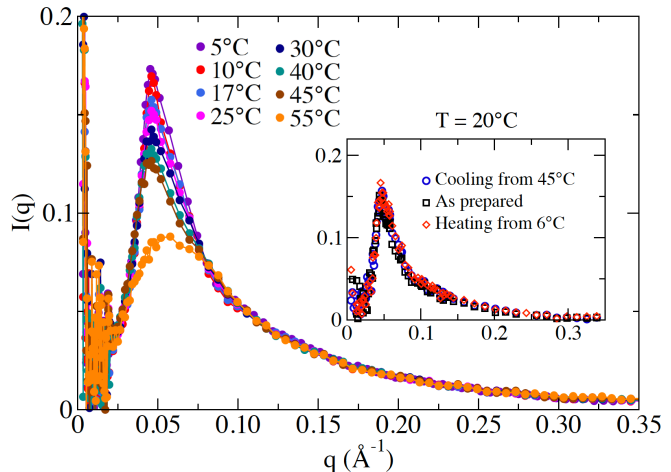


FIG. 4. SANS: Sample $c = 21 \text{ mg ml}^{-1}$. $I(q)$ in the q -range from $0.0025 < q < 0.35 \text{ \AA}^{-1}$ (normalized to coincide with the normalized form factor at large q) at temperatures varying from 55°C to 5°C , measured at the D22 diffractometer. The inset (same units) shows three different measurements done at the PACE diffractometer, all performed at 20°C to provide evidence of full reversibility. The sample was initially measured at 20°C after a long equilibration (black squares). Subsequently the sample was re-measured at 20°C during a cooling scan started from 45°C (blue circles) and finally re-measured at 20°C during a heating scan starting from 6°C (red diamonds).

value for α has been determined by imposing that in the $0.1 < q < 0.3 \text{ \AA}^{-1}$ region the signal from NSs coincides (again apart from the constant β) with the normalized theoretical form factor $P(q)$, by defining

$$\left(\frac{d\sigma_c}{d\Omega} \right)_{NS}(q) = I_m(q) - \alpha I_s(q) \quad (7)$$

and finding α and β by minimizing the variance χ^2

$$\chi^2 \equiv \int_{q=0.1}^{q=0.3} \left[\left(\frac{d\sigma_c}{d\Omega} \right)_{NS}(q) - \beta P(q) \right]^2 dq$$

The best fit values for α are all between 0.99 and 0.96, suggesting a very small temperature variation of the solvent scattering. The best fit values of β (defining the value of the form factor in $q = 0$) are found to be $1.4 \leq \beta \leq 1.8$.

Figure 4 shows the resulting $I(q)$ (normalized by β) at all investigated temperatures. According to these results, we can differentiate three scattering regions. At low- q values, at the lower limit of the experimental resolution, we observe a significant signal, suggesting the presence of correlated scatterers over tens of nanometers. This upturn for $q < 0.02 \text{ \AA}^{-1}$, which is commonly found in polyelectrolyte solutions^{47,48}, has been widely discussed by several authors^{42,49–53}. Within this context, the strong

low- q signal is usually associated to the recurrent clustering behavior of biological macromolecules^{54–57}. In the present case, this tendency is always observed, at all T , even when all NS are not bounded and hence this very low q peak can not be associated with inhomogeneities in the gel. We note on passing that DLS has also evidenced the presence of small concentrations of approx $0.1 \mu\text{m}$ size, which are possibly introduced in the sample during the DNA synthesis. These impurities could be well responsible for this low q signal.

The most interesting part of the scattered intensity is the region $q \approx 0.05 \text{ \AA}^{-1}$, where we observe the presence of a peak which increases its amplitude on cooling. The corresponding real-space distance, estimated as $d^* = 2\pi/q = 114 \text{ \AA}$ is comparable with the center-to-center distance in a pair of bonded NSs (estimated in about 140 \AA), suggesting the possibility to interpret such growth as structural evidence of the progressive formation of the gel, in agreement with the previous DLS measurements of the same DNA NS sample solutions¹⁷.

For $q > 0.1 \text{ \AA}^{-1}$ the intensity does not vary with temperature anymore and all the curves decay following the form factor.

It is worth noting that the aggregation process of the DNA NSs is fully reversible. This is clearly visible in the inset of Fig. 4, where three measurements at $T = 20^\circ\text{C}$ are reported. The first measurement was taken at the sample preparation conditions, whereas the second and third were acquired, always at 20°C , after cooling the sample down from $T = 45^\circ\text{C}$ and after heating it up from $T = 6^\circ\text{C}$, respectively.

C. Structure Factor Analysis

Assuming the possibility of decoupling the center of mass from the orientational variables, it is customary to approximate $I(q)$ (Eq. 5) as

$$I(\mathbf{q}) = P(\mathbf{q}) + \frac{1}{N_S} \left\langle \sum_{l=1}^{N_S} \sum_{\substack{m=1 \\ m \neq l}}^{N_S} \exp[i\mathbf{q} \cdot (\mathbf{r}_{CM}^l - \mathbf{r}_{CM}^m)] \right\rangle \langle F_l(\mathbf{q}) F_m^*(\mathbf{q}) \rangle \quad (8)$$

Defining the center-to-center structure factor $S(q)$

$$S(\mathbf{q}) - 1 \equiv \frac{1}{N_S} \left\langle \sum_{l=1}^{N_S} \sum_{\substack{m=1 \\ m \neq l}}^{N_S} \exp[i\mathbf{q} \cdot (\mathbf{r}_{CM}^l - \mathbf{r}_{CM}^m)] \right\rangle \quad (9)$$

and considering the previous definitions for $P(\mathbf{q})$ and $F(\mathbf{q})$ one can write

$$I(\mathbf{q}) = P(\mathbf{q}) + [S(\mathbf{q}) - 1]F(\mathbf{q}) \quad (10)$$

In the limit of non-interacting particles, $S(\mathbf{q}) = 1$ and $I(\mathbf{q})$ provides a measure of the form factor $P(\mathbf{q})$. The

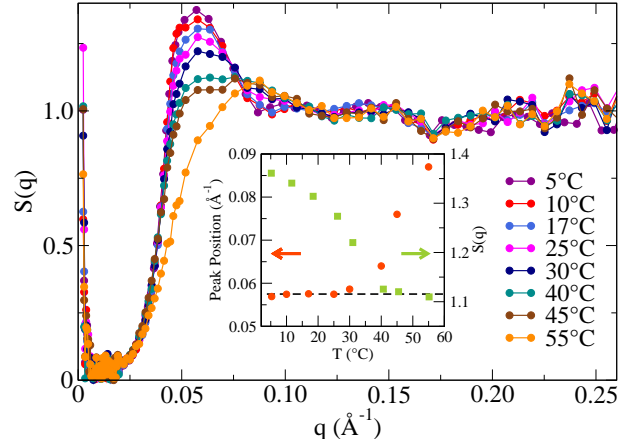


FIG. 5. Static structure factor $S(q)$ at different temperatures ($55-5^\circ\text{C}$) calculated from the ratio between $I(q)$ and $P_{sim}(q)$. The shift of the peak position (\AA^{-1}) (dark orange dots) and its intensity (light green squares) as a function of temperature are displayed in the inset.

measured form factor is sufficient to evaluate $S(\mathbf{q})$, if the approximation $F(\mathbf{q}) = P(\mathbf{q})$ is valid in the region where $S(\mathbf{q}) \neq 1$. In this further case

$$I(\mathbf{q}) = S(\mathbf{q})P(\mathbf{q}) \quad (11)$$

Since we have access to the atomic coordinates in the numerical study, we can evaluate both $P(\mathbf{q})$ and $F(\mathbf{q})$, both reported in Fig. 2, to be used in conjunction with the experimental $I(\mathbf{q})$ for extracting $S(\mathbf{q})$, according to Eq. 10 and Eq. 11. The resulting structure factor has to be considered as an experimentally accessible effective structure factor, since it still depends on the decoupling approximation between positions and orientation and the decoupling of the orientation between different pairs. For both routes (Eq. 10 and Eq. 11) we find a consistent $S(\mathbf{q})$ prediction, even if the approximation $S(\mathbf{q}) = I(\mathbf{q})/P(\mathbf{q})$ is preferred since it does not suffer from numerical errors associated to the ratio between small numbers, encountered at large q when using $S(\mathbf{q}) = 1 + [I(\mathbf{q}) - P(\mathbf{q})]/F(\mathbf{q})$.

Fig. 5 shows the effective structure factor,

$$S(q) = \frac{I(q)}{\beta P(q)}$$

where, once more, $P(q)$ is the normalized form factor and β the form factor value at the origin. The T -dependence of the effective structure factor shows the onset of a peak at a q^{peak} position that shifts to lower q values (see inset of Fig. 5) as the temperature decreases until it stabilizes at $q^{peak} = 0.0585 \text{ \AA}^{-1}$ ($2\pi/q^{peak} = 107.4 \text{ \AA}$) once the gel is formed. $S(q^{peak})$ increases slower and slower on cooling. This behavior, predicted theoretically and supported by numerical calculations has been observed in the

ageing process of a clay gel⁵⁸ but never observed experimentally in a controlled and designed thermoreversible system. In the theoretical studies, saturation results from the formation of a fully bonded network of tetravalent particles. In this "ground zero" structure, all possible bonds are essentially formed and structural evolution is completed. Dynamics is still possible via the rare breaking and reforming of the inter-NS bonds on a timescale dictated by the free-energy cost $\Delta G_{breaking}$. This last quantity has been estimated by DLS experiments to be about $1.3 \Delta G_{CGATCG}$ where ΔG_{CGATCG} is the known⁵⁹ binding free energy of the sticky CGATCG sequence. At the lowest investigate T , the bond-breaking timescale is larger than 10 seconds. Fig. 5 also shows that the system has a very small compressibility (the limit of $S(q)$ for $q \rightarrow 0$), as expected for a solution of significantly charged particle at small ionic strength⁶⁰.

V. CONCLUSIONS

We have investigated the aggregation process of self-assembled DNA NSs, generated by mixing equimolar quantities of four properly designed 49-bases DNA oligomers. On cooling, these four strands first associate to form a four-arms star with sticky ends, followed by aggregation of these four-functional supramolecules in a thermoreversible gel structure. The dynamics and phase behavior of this interesting biomaterial have been previously investigated via light scattering.

Here, we provided a structural characterization of the system, resulting from to the synergy between experiments and computer simulations.

Specifically, we reported the first SANS measurement of the form factor and compared it with predictions based on oxDNA2²⁹, a recently developed coarse grained model for investigating DNA nanotechnology. The predictions of the model are found to be in very good agreement with the experimental results in the entire wavevector range, allowing us to estimate precisely the shape of the NS. For the investigated low salt concentration, the NS is found to be rather planar, a geometry that minimizes the electrostatic repulsions. Simulations also provide evidence that the T effect on the shape is negligible. By contrast, the ionic strength exerts a strong dependence on the shape of the NS. On increasing salt concentration, the gyration radius significantly decreases and the four arms fluctuate more freely.

SANS measurements in the equilibrium gel region showed the presence of a peak in the scattered intensity whose amplitude evolves during the aggregation process and appears to level off at the lowest investigated T s, suggesting that a structurally complete fully bonded tetrahedral network has been formed. The effective structure factor, evaluated assuming the validity of the relation $S(q) = I(q)/P(q)$, confirms the previous analysis, in agreement with theoretical predictions of simplified colloidal patchy-particle models⁶¹. Unfortunately, low ionic-

strength simulations of the aggregation process with an accurate DNA model, even at the coarse grained oxDNA2 level, are still unfeasible and a direct comparison between simulations and experiments in the gel phase is still lacking. Hopefully, a new experiment at significantly large ionic strength (where bulk simulations start to be feasible⁶²) will allow us to clarify the dependence of the structural properties and the ionic strength effect on the gel structure. Additional experiments could also assess the validity of the decoupling between translational and orientational correlations and substantiate the interpretation of the effective $S(q)$ as the center-to-center structure factor.

SANS techniques have often been applied to the study of gels composed by polymers^{63–65} (mostly irreversibly cross-linked^{66–70}), proteins^{71–73} or nanocomposite clays^{58,74–76}, but only rarely interpreted in terms of form and structure factors even for chemical gels very similar to the present physical one (e.g. the binary system developed by the group of Shibayama based on two four-arm poly(ethylene glycol) polymers^{20,77}). The DNA gel discussed here, built on the base-pair selectivity, represents a realisation of an ideal biocompatible physical gel free of entanglement and defects and with a well defined supramolecular unit. Such monodisperse constituents of the network nodes, together with the possibility to compare the neutron data with the accurate geometry provided by the simulations, is crucial for evaluating an effective gel structure factor.

Acknowledgments

FS and JFC acknowledge support from ETN-COLLDENSE (H2020-MCSA-ITN-2014, Grant No. 642774). FS, TB, FB acknowledge support from MIUR-PRIN. LR acknowledges support from the Austrian Research Fund (FWF) through the Lise-Meitner Fellowship M 1650-N27, and from the European Commission through the Marie Skłodowska-Curie Fellowship 702298-DELTAS.

We also acknowledge ILL, LLB and the HZB for beam-time allocation and the support on data analysis. This project has received funding from the European Union's Seventh Framework Programme for research, technological development and demonstration under the NMI3-II Grant number 283883.

Additional Information

Competing financial interests: the authors declare no competing financial interests.

¹M. Yoshida, and J. Lahann, ACS Nano **26**, 1101–1107 (2008).

²A. Condon, Nat. Rev. Genet. **7**, 565–575 (2006).

³M. Patil, D. S. Mehta, and S. Guvva, J. Indian Soc. Periodontol. **12** (2008).

⁴P. C. Nicolson, and J. Vogh, Biomaterials **22**, 3273–3283 (2001).

- ⁵N. A. Peppas, J. Z. Hilt, A. Khademhosseini, and R. Langer, *Adv. Mater.* **18**, 1345–1360 (2006).
- ⁶J. Kopeček, *Eur. J. Pharm. Sci.* **20**, 1–16 (2003).
- ⁷D. Costa, A. J. M. Valente, M. Graça Miguel, and J. Queiroz, *Colloids Surf., A* **442**, 181–190 (2014).
- ⁸D. Tada, T. Tanabe, A. Tachibana, and K. Yamauchi, *J. Biosci. Bioeng.* **100**, 551–555 (2005).
- ⁹A. J. Steckl, *Nature Photon.* **1**, 3–5 (2007).
- ¹⁰A. J. Steckl, H. Spaeth, H. You, E. Gomez, and J. Grote, *Opt. Photonics News* **22**, 34–39 (2011).
- ¹¹D. Boneh, C. Dunworth, R. J. Lipton, and J. I. Sgall, *Discrete Appl. Math.* **71** (1996).
- ¹²S. M. Douglas, I. Bachelet, and G. M. Church, *Science* **335**, 831–834 (2012).
- ¹³N. C. Seeman, *Nature* **421**, 427–431 (2003).
- ¹⁴Y. W. Kwon, C. H. Lee, D. H. Choi, and J. I. Jin, *J. Mater. Chem.* **19**, 1353–1380 (2009).
- ¹⁵R. M. Zadeegan and M. L. Norton, *Int. J. Mol. Sci.* **13**, 7149–7162 (2012).
- ¹⁶S. Biffi, R. Cerbino, F. Bomboi, E. M. Paraboschi, R. Asselta, F. Sciortino, and T. Bellini, *Proc. Natl. Acad. Sci. USA* **110**, 15633–15637 (2013).
- ¹⁷S. Biffi, R. Cerbino, G. Nava, F. Bomboi, F. Sciortino, and T. Bellini, *Soft Matter* **11** (2015).
- ¹⁸E. Bianchi, J. Largo, P. Tartaglia, E. Zaccarelli, and F. Sciortino, *Phys. Rev. Lett.* **97**, 168301 (2006).
- ¹⁹P. J. Lu, E. Zaccarelli, F. Ciulla, A. B. Schofield, F. Sciortino, and D. A. Weitz, *Nature* **453** (2008).
- ²⁰T. Sakai, T. Matsunaga, Y. Yamamoto, C. Ito, R. Yoshida, S. Suzuki, N. Sasaki, and M. Shibayama, *Macromolecules* **41**, 5379–5384 (2008).
- ²¹F. Bomboi, S. Biffi, R. Cerbino, T. Bellini, F. Bordi, and F. Sciortino, *Eur. Phys. J. E Soft Matter* **38**, 1–8 (2015).
- ²²J. P. Doye, T. E. Ouldridge, A. A. Louis, F. Romano, P. Šulc, C. Matek, B. E. Snodin, L. Rovigatti, J. S. Schreck, R. M. Harrison, *et al.*, *Phys. Chem. Chem. Phys.* **15**, 20395–20414 (2013).
- ²³P. Desjardins, and D. Conklin, *J. Vis. Exp.* **45** (2010).
- ²⁴C. D. Dewhurst, *Meas. Sci. Technol.* **19** (2008).
- ²⁵<http://www.ill.fr/D22/>.
- ²⁶C. Dewhurst, ILL (2003).
- ²⁷U. Keiderling, and A. Wiedenmann, *Physica B* **213–214**, 895–897 (1995).
- ²⁸U. Keiderling, *Appl. Phys. A* **74** (2002).
- ²⁹B. E. Snodin, F. Randisi, M. Mosayebi, P. Šulc, J. S. Schreck, F. Romano, T. E. Ouldridge, R. Tsukanov, E. Nir, A. A. Louis, *et al.*, *J. Chem. Phys.* **142**, 234901 (2015).
- ³⁰T. E. Ouldridge, A. A. Louis, and J. P. Doye, *J. Chem. Phys.* **134**, 085101 (2011).
- ³¹P. Šulc, F. Romano, T. E. Ouldridge, L. Rovigatti, J. P. Doye, and A. A. Louis, *J. Chem. Phys.* **137**, 135101 (2012).
- ³²<https://www.ncnr.nist.gov/resources/n-lengths/>.
- ³³S.-H. Chen and P. Tartaglia, *Scattering Methods in Complex Fluids* (Cambridge University Press, 2015).
- ³⁴M. Kotlarchyk and S.-H. Chen, *J. Chem. Phys.* **79**, 2461–2469 (1983).
- ³⁵R. A. Jones, *Soft condensed matter*, Vol. 6 (Oxford University Press, 2002).
- ³⁶K. Kassapidou, W. Jesse, M. Kuil, A. Lapp, S. Egelhaaf, and J. Van der Maarel, *Macromolecules* **30**, 2671–2684 (1997).
- ³⁷A. Guinier, and G. Fournet, *Small angle scattering of X-rays*.
- ³⁸J. R. C. van der Maarel, and K. Kassapidou, *Macromolecules* **31**, 5734–5739 (1998).
- ³⁹J. R. C. van der Maarel, *Biophys. J.* **76**, 2673–2678 (1999).
- ⁴⁰H. Lederer, R. P. May, J. K. Kjems, and H. Heumann, *Eur. J. Biochem.* **161**, 191–196 (1986).
- ⁴¹J. D. Watson, and F. H. C. Crick, *Nature* **171**, 737–738 (1953).
- ⁴²R. Borsali, H. Nguyen, and R. Pecora, *Macromolecules* **31**, 1548–1555 (1998).
- ⁴³V. Luzzati, F. Masson, A. Mathis, and P. Saludjian, *Biopolymers* **4** (1976).
- ⁴⁴J. Garcia de la Torre, and A. Horta, *J. Phys. Chem.* **80** (1976).
- ⁴⁵M. H. J. Koch, Z. Sayers, P. Sicre, and D. Svergun, *Macromolecules* **28** (1995).
- ⁴⁶J.-P. Hansen and I. R. McDonald, *Theory of simple liquids* (Elsevier, 1990).
- ⁴⁷M. Milas, M. Rinaudo, R. Duplessix, R. Borsali, and P. Lindner, *Macromolecules* **28**, 3119–3124 (1995).
- ⁴⁸N. Arfin, V. K. Aswal, J. Kohlbrecher, and H. B. Bohidar, *Polymer* **65**, 175–182 (2015).
- ⁴⁹M. Sedlak, *J. Chem. Phys.* **105**, 10123–10133 (1996).
- ⁵⁰M. Shibayama, *Macromol. Chem. Phys.* **199**, 1–30 (1998).
- ⁵¹H. Matsuoka, D. Schwahn, and N. Ise, *Macromolecules* **24** (1991).
- ⁵²Y. Zhang, J. F. Douglas, B. D. Ermi, and E. J. Amis, *J. Chem. Phys.* **114**, 3299–3313 (2001).
- ⁵³M. Sedlak, *J. Chem. Phys.* **116**, 5256–5262 (2002).
- ⁵⁴K. Dusek, and W. Prins, *Adv. Polym. Sci.* **6** (1969).
- ⁵⁵E. Geissler, A. Hecht, and R. Duplessix, *J. Polym. Sci. Part B Polym. Phys.* **20** (1982).
- ⁵⁶E. Geissler, F. Horkay, and A. Hecht, *Phys. Rev. Lett.* **71** (1993).
- ⁵⁷J. M. Guenet, M. Kein, and A. Menelle, *Macromolecules* **22** (1989).
- ⁵⁸B. Ruzicka, E. Zaccarelli, L. Zulian, R. Angelini, M. Sztucki, A. Moussaïd, T. Narayanan, and F. Sciortino, *Nat. Mater.* **10**, 56–60 (2011).
- ⁵⁹J. SantaLucia, *Proc. Natl. Acad. Sci. USA* **95**, 1460–1465 (1998).
- ⁶⁰J. R. Van der Maarel, *Introduction to biopolymer physics* (World Sci., 2008).
- ⁶¹F. Sciortino and E. Zaccarelli, *Curr. Opin. Solid St. M.* **15**, 246–253 (2011).
- ⁶²L. Rovigatti, F. Bomboi, and F. Sciortino, *J. Chem. Phys.* **140** (2014).
- ⁶³L. Z. Rogovina, V. G. Vasil’ev, and E. E. Braudo, *Polym. Sci. Ser. C* **50**, 85–92 (2008).
- ⁶⁴T. Rossow, and S. Seiffert, *Polym. Chem.* **5**, 3018–3029 (2014).
- ⁶⁵S. Chaterji, I. K. Kwon, and K. Park, *Prog. Polym. Sci.* **32**, 1083–1122 (2007).
- ⁶⁶T. Matsunaga, T. Sakai, Y. Akagi, U. il Chung, and M. Shibayama, *Macromolecules* **42**, 6245–6252 (2009).
- ⁶⁷L. H. Lee, Xerox Corp. Plenum Press, 1st ed., 483–495 (1989).
- ⁶⁸H. Benoit, D. Decker, C. Duplessix, C. Picot, and P. Rempp, *J. Polym. Sci. Part B Polym. Phys.* **14**, 2199–2128 (1976).
- ⁶⁹R. Ullman, *Macromolecules* **15**, 1395–1402 (1982).
- ⁷⁰H. M. Tsay, and R. Ullman, *Macromolecules* **21**, 2963 (1988).
- ⁷¹A. M. Jonker, D. W. P. M. Löwik, and J. C. M. van Hest, *Chem. Mater.* **24**, 759–773 (2012).
- ⁷²J. D. Ehrick, S. K. Deo, T. W. Browning, L. G. Bachas, M. J. Madou, and S. Daunert, *Nat. Mater.* **4**, 298–302 (2005).
- ⁷³S. Tang, M. Wang, and B. D. Olsen, *J. Am. Chem. Soc.* **137**, 3946–3957 (2015).
- ⁷⁴P. Li, Siddaramaiah, N. H. Kim, S. B. Heo, and J. H. Lee, *Composites Part B* **39**, 756–763 (2008).
- ⁷⁵C. W. Chang, A. Van Spreeuwel, C. Zhang, and S. Varghese, *Soft Matter* **6**, 5157–5164 (2010).
- ⁷⁶L. Z. Zhao, C. H. Zhou, J. Wang, D. S. Tong, W. H. Yu, and H. Wang, *Soft Matter* **11**, 9229–9246 (2015).
- ⁷⁷M. Shibayama, *Polym. J.* **43** (2011).